Clinicopathologic and Genomic Characterization of Inflammatory Myofibroblastic Tumors of the Head and Neck

Highlighting a Novel Fusion and Potential Diagnostic Pitfall

Darcy A. Kerr, MD,† Lester D.R. Thompson, MD,‡ Laura J. Tafe, MD,*† Vickie Y. Jo, MD,§ Azfar Neyaz, MD,‖ Prashanthi Divakar, MD,¶ Joseph A. Paydarfar, MD,†¶ David A. Pastel, MD,†# Keisuke Shirai, MD, MSc,†** Ivy John, MD,†† Raja R. Seethala, MD,†† Claudia M. Salgado, MD, PhD,‡‡ Vikram Deshpande, MD,‖ Julia A. Bridge, MD,§§‖‖ Karl Kashofer, PhD,¶¶ Iva Brčić, MD,¶¶ and Konstantinos Linos, MD*†*

Abstract: Inflammatory myofibroblastic tumor (IMT) is a distinctive fibroblastic and myofibroblastic spindle cell neoplasm with an accompanying inflammatory cell infiltrate and frequent receptor tyrosine kinase activation at the molecular level. The tumor may recur and rarely metastasizes. IMT is rare in the head and neck region, and limited information is available about its clinicopathologic and molecular characteristics in these subsites. Therefore, we analyzed a cohort of head and neck IMTs through a multi-institutional approach. Fourteen cases were included in the provisional cohort, but 1 was excluded after molecular analysis prompted reclassification. Patients in the final cohort included 7 males and 6 females, with a mean age of 26.5 years. Tumors were located in the larynx (n = 7), oral cavity (n = 3), pharynx (n = 2), and mastoid (n = 1). Histologically, all tumors showed neoplastic spindle cells in storiform to fascicular patterns with associated chronic inflammation, but the morphologic spectrum was wide, as is characteristic of IMT in other sites. An underlying fusion gene event was identified in 92% (n = 11/12) of cases and an additional case was ALK-positive by IHC but could not be evaluated molecularly. *ALK* represented the driver in all but 1 case. Rearrangement of *ALK*, fused with the *TIMP3* gene (n = 6) was most commonly detected, followed by 1 case each of the following fusion gene partnerships: *TPM3-ALK*, *KIF5B-ALK*, *CARS-ALK*, *THBS1-ALK*, and a novel alteration, *SLC12A2-ROS1*. The excluded case was reclassified as spindle cell rhabdomyosarcoma after detection of a *FUS-TFCP2* rearrangement and retrospective immunohistochemical confirmation of rhabdomyoblastic differentiation, illustrating an important diagnostic pitfall. Two IMT patients received targeted therapy with crizotinib, with a demonstrated radiographic response. One tumor recurred but none metastasized. These results add to the growing body of evidence that kinase fusions can be identified in the majority of IMTs and that molecular analysis can lead to increased diagnostic accuracy and broadened therapeutic options for patients.

Key Words: inflammatory myofibroblastic tumor, head and neck, mesenchymal neoplasms, soft tissue tumors, ALK immunohistochemistry, ROS1

(*Am J Surg Pathol* 2021;45:1707–1719)

From the Departments of *Pathology and Laboratory Medicine; #Radiology; **Medical Oncology; ¶Section of Otolaryngology, Dartmouth-Hitchcock Medical Center, Lebanon; †Geisel School of Medicine at Dartmouth, Hanover, NH; ‡Department of Pathology, Southern California Permanente Medical Group, Woodland Hills, CA; §Department of Pathology, Brigham and Women's Hospital and Harvard Medical School; ‖Department of Pathology, Massachusetts General Hospital and Harvard Medical School, Boston, MA; ††Department of Pathology, University of Pittsburgh; ‡‡Department of Pathology, Children's Hospital of Pittsburgh, Pittsburgh, PA; §§Molecular Division, ProPath LLC, Dallas, TX; ‖‖Department of Pathology and Microbiology, University of Nebraska Medical Center, Omaha, NE; and ¶¶Diagnostic and Research Institute of Pathology, Medical University of Graz, Graz, Austria.

Conflicts of Interest and Source of Funding: NGS studies were supported by internal research funding from the D&R Institute of Pathology, Medical University of Graz, Austria. The authors have disclosed that they have no significant relationships with, or financial interest in, any commercial companies pertaining to this article.

Correspondence: Darcy A. Kerr, MD, Dartmouth-Hitchcock Medical Center, Department of Pathology, One Medical Center Drive, Borwell Level 4, Lebanon, NH 03756 (e-mail: darcy.a.kerr@hitchcock.org).

Inflammatory myofibroblastic tumor (IMT) is a distinctive fibroblastic/myofibroblastic neoplasm that harbors a chronic inflammatory cell infiltrate of lymphocytes, plasma cells, and/or eosinophils.[1] Most IMTs occur in the first 3 decades of life (mean age = 10 y), although cases can occur throughout adulthood. IMTs occur throughout the body, most frequently involving the lung, abdomen/pelvis, and retroperitoneum. Symptoms depend on the site of involvement.[1,2] Approximately 14% to 18% of extrapulmonary IMTs involve the head and neck region, most commonly the orbit and upper airways including the larynx.[3,4] About 25% of extrapulmonary IMTs recur locally, partially related to anatomic considerations, whereas metastasis is rare (< 5%); lung, brain, liver, and

bone are the reported sites of metastatic spread.[1,5] Reliable prognostic indicators for conventional IMT are lacking.[1,6,7]

IMT has historically been included within the rubric of *inflammatory pseudotumor*, a descriptive term applied to numerous neoplastic and non-neoplastic processes.[6] However, molecular analysis has helped distinguish IMT as a distinctive neoplasm largely characterized by receptor tyrosine kinase (RTK) activation. Overall, 50% to 70% contain rearrangements of the anaplastic lymphoma kinase (*ALK*) gene on chromosome 2p23. The correlation with age is robust, with 80% to 90% of pediatric IMTs demonstrating a fusion.[8,9] Rearrangements involve an ever-expanding list of partner genes, including *TPM3*, *TPM4*, *CLTC*, *RANBP2*, *ATIC*, *CARS*, *SEC 31A*, *SEC 31L1*, *EML4*, *TFG*, and *FN1*, among others.[1,2] In patients above 40 years of age at presentation, *ALK* rearrangements are uncommon.[1] Although ALK-negative tumors may be more likely to metastasize, ALK status does not correlate with recurrence risk in conventional IMT.[4,6,7] The presence of a clonal *ALK* rearrangement generally correlates with reactivity for ALK immunohistochemistry (IHC).[6,10,11] Alternatively, rearrangements of *ROS1*, *PDGFRB*, *NTRK3*, *ETV6*, *IGFR1*, and *RET* have also been implicated as driver mutations in subsets of IMTs,[12,13] such that the majority of IMTs harbor kinase fusions, ranging from 68%[8] to 85%.[2] While surgical excision is the mainstay of treatment for IMT, targeted molecular therapy via RTK inhibition may be applied in certain clinical scenarios with variable effectiveness.[2,14] Overall, IMTs are relatively rare within the head and neck region, and whether IMTs in this site have distinctive features is not specifically reported. Therefore, a multi-institutional study was undertaken to define the clinical, morphologic, immunohistochemical, and genetic features of a large case series.

MATERIALS AND METHODS

Fourteen candidate IMTs were identified from the archives of 6 collaborating institutions (Dartmouth-Hitchcock Medical Center, Lebanon, NH; Southern California Permanente Medical Group, Woodland Hills, CA; Brigham and Women's Hospital, Boston, MA; Massachusetts General Hospital, Boston, MA; University of Pittsburgh, Pittsburgh, PA; Children's Hospital of Pittsburgh, Pittsburgh, PA) after Institutional Review Board approval. Tracheal tumors were considered as part of the lung/respiratory system for purposes of this study and excluded. Available hematoxylin and eosin (H&E)-stained and IHC slides were reviewed to confirm the diagnosis. Clinical and radiographic information was obtained from the electronic medical records. Additional IHC and/or molecular analysis was performed in select cases. One case was reclassified after molecular analysis revealed a *FUS-TFCP2* fusion (see below), leading to a final cohort of 13 IMTs.

Pathologic Examination

Specimens were fixed in formalin, routinely processed, and embedded in paraffin. Available H&E-stained slides (range: 1 to 16) were reviewed and assessed for histologic features including tumor margin (ill-defined vs. well-defined), mitotic index (mitoses per 2 mm^2), percent neoplastic cellularity (2-dimensional area occupied by spindle cells based on H&E slide review, supplemented by IHC), predominant inflammatory component (lymphocytes, plasma cells, eosinophils, histiocytes), the extent of inflammation (diffuse, occupying $\geq 50\%$ of the tumor surface; limited, $< 50\%$), and density of inflammation (3+, evident at ×4; 2+, evident at ×10; 1+; evident at ×20, using standard ×10 ocular).[15] The presence or absence of the following features was recorded: surface ulceration, atypical mitotic figures, necrosis, lymphovascular invasion, ganglion-like cells, granular cell change, intranuclear inclusions, and marked pleomorphism. Each tumor was classified according to the relative proportion of each of the 3 previously described, frequently commingled histologic patterns: myxoid, compact spindle cell, or dense collagenous.[4] The myxoid pattern was characterized by loose spindle cells in a myxoid or edematous background with prominent vasculature, reminiscent of nodular fasciitis. The compact spindle cell pattern demonstrated a densely cellular spindle cell proliferation in storiform and fascicular arrangements. The dense collagenous pattern was relatively hypocellular, composed of collagen with few spindle cells, similar to scar or fibromatosis.[4,6,15]

Immunohistochemistry

IHC studies interpreted at the time of original diagnosis were reviewed and recorded. The following IHC antibodies were performed: ALK, ROS1, smooth muscle actin (SMA), muscle-specific actin (MSA), desmin, pancytokeratin, p63, S100 protein, and CD34. Additional studies were performed on 4-μm formalin-fixed, paraffin-embedded (FFPE) tissue sections using a Leica BOND-III (Leica Biosystems, Buffalo Grove, IL) automated IHC stainer with appropriate positive and negative controls. Several different ALK antibodies were used based on institutional preference.

Fluorescence In Situ Hybridization

Fluorescence in situ hybridization (FISH) was performed on 4-μm FFPE tissue sections for rearrangement of the *ALK* or *ROS1* gene loci. FISH was performed using standard protocols with break-apart probes for the 5′ and 3′ regions of the *ALK* gene at 2p23 (Abbott Laboratories, Chicago, IL) or *ROS1* gene at 6q22 (Agilent, Santa Clara, CA). Slide adequacy and signal enumeration were evaluated and satisfactory for both control and patient slides. The results of these analyses were based on the enumeration of interphase nuclei with strong, well-delineated signals from nonoverlapping tumor cells. The orange-green split signals and the single orange signal (with loss of the 5′ green signal) were counted as rearranged patterns. A minimum of 50 cells were counted by 2 observers for *ALK* and 200 for *ROS1*. An orange-green split signal or isolated orange signal (loss of 5′ green signal) were scored as rearranged patterns. The cutoff level for scoring as rearranged was $\geq 15\%$ abnormal nuclei for both *ALK* and *ROS1*, based on in-house validation studies.

Next-generation Sequencing Assays

Archer FusionPlex NGS: RNA Extraction, Sequencing, and Analysis

Molecular analysis (fusion gene detection) was performed on FFPE material using next-generation sequencing (NGS)-based anchored multiplex polymerase chain reaction technique. Cases with available material underwent RNA-based analysis with Archer FusionPlex Sarcoma Panel v4 (11 cases) or v5 (1 case) to assess specific rearrangements in 37 genes (*ALK*, *BCOR*, *BRAF*, *CAMTA1*, *CCNB3*, *CHMP2a*, *CIC*, *EPC1*, *EWSR1*, *FOS*, *FOSB*, *FOXO1*, *FUS*, *GLI1*, *HMGA2*, *JAZF1*, *MEAF6*, *MKL2*, *NCOA2*, *NTRK1*, *NTRK2*, *NTRK3*, *PAX3*, *PDGFB*, *PLAG1*, *RAB7a*, *ROS1*, *SS18* (*SYT*), *STAT6*, *TAF15*, *TCF12*, *TFE3*, *TFG*, *TGFBR3*, *USP6*, *VCP*, and *YWHAE*) or 40 genes (those previously listed plus *KMT2a*, *MGEA5*, and *RET*), respectively. For each sample, 5 to 8, 10-μm FFPE sections were cut from a representative block, and macrodissection was performed with a scalpel to enrich for tumor content. RNA was isolated using the Maxwell RSC RNA FFPE kit (Promega, Madison, WI), according to the manufacturer's instructions. RNA was quantified by ribogreen fluorescence, and 250 ng total RNA was used for the Archer FusionPlex Sarcoma Kit. NGS libraries were sequenced on Ion Torrent Proton using the Ion PI Hi-Q Sequencing 200 kit (Thermo Fischer, Waltham, MA). The analysis was performed with ArcherDX Analysis software, Version 5.1.3.

Whole-transcriptome NGS; RNA-seq Library Preparation, Sequencing, and Analysis

The KAPA RNA HyperPrep Kit with RiboErase from Roche (Indianapolis, IN) was used to construct a stranded RNA-seq library in duplicate for Illumina sequencing, according to the supplier's recommendation. Briefly, 100 ng of RNA isolated from an FFPE tissue section (10-μm thick) of the tumor tissue using an AllPrep DNA/RNA Mini Kit (Qiagen, Hilden, Germany) was depleted of rRNA and fragmented. Following the first and second-strand cDNA synthesis and adapter ligation, the libraries were amplified. After library amplification, Agilent 2200 TapeStation system was used for quality control. The libraries were quantified with KAPA Library Quantitation Kit before normalization and pooling before sequencing on HiSeq. 2500 (Illumina, San Diego, CA) instrument in rapid run mode generating a minimum of 100 million 2×101 paired-end reads per sample. Raw sequencing data were converted to FASTQ files using Illumina's bcl2fastq software (v2.20.0.422). FASTQs files were used as input to STAR-Fusion, version 1.2.0 to identify putative fusion transcripts.[16] Candidate fusions were filtered with FusionInspector (part of the STAR-Fusion package), using default parameters. The fusion event detected by this method was also detected as a structural translocation at the DNA level following DNA extraction (AllPrep DNA/RNA Mini Kit; Qiagen), library preparation (custom xGen target capture to include shearing, purification, adaptor ligation, and polymerase chain reaction amplification), and whole-exome NGS.

RESULTS

Clinical and Pathologic Characteristics

Patients included 7 males and 6 females, with a mean age of 26.5 years (median = 26 y, range: 7 to 69 y). Tumors were located in the larynx (n = 7), oral cavity (n = 3), pharynx (n = 2), and mastoid bone (n = 1). The most common presenting symptom was hoarseness, experienced in 6 patients with laryngeal tumors, and 1 each with a hypopharynx and tongue tumor, respectively. Other presenting symptoms included loss of voice (n = 3), changes in hearing (n = 2), cough (n = 2), noting a mass (n = 2), dysphagia (n = 1), and hemoptysis (n = 1). Length of symptoms ranged from 0.5 to 960 months before the presentation (n = 11; unavailable for 2). There was no history of radiation exposure or other benign or malignant tumor. For patients where history was available, 40% (4/10) used alcohol, whereas tobacco use was uncommon (1/10). Preoperative imaging studies, when available (n = 7), showed enhancing, lobulated, pedunculated, sometimes exophytic masses that were well or poorly demarcated. The average tumor size was 2.2 cm (range: 0.6 to 10.6 cm; median = 1.5 cm). One case was cystic (case 4) and 1 showed calcification with posterior cricoid cartilage erosion, prompting concern for malignancy (case 8; Figs. 1A–C). Clinical characteristics are outlined in Table 1.

The material received included 15 specimens (8 excisional biopsies, 6 incisional biopsies, 1 resection) from the primary tumors of 13 patients. The initial biopsy in 1 patient was interpreted as traumatic fibroma (case 9). Another patient had incisional biopsy followed by crizotinib treatment and subsequent excision (case 8; Fig. 1D). No tumor as multifocal. When the interface with adjacent nonlesional tissue could be assessed, approximately half of the tumors had a well-demarcated margin (4/7), while an infiltrative margin was seen in the remaining tumors (Fig. 2). Histologically, the lesional spindle cells were arranged in storiform to fascicular patterns, and all cases demonstrated a storiform pattern at least focally. The compact and myxoid patterns predominated in 9 and 3 cases, respectively, whereas in 1 case an equal mixture of the aforementioned patterns was observed. One case with a compact pattern showed intense inflammation which largely obscured the underlying minor storiform spindle cell component (case 12), previously published as a part of a series of IMT demonstrating morphologic overlap with immunoglobulin (Ig) G_4-related disease.[17] The neoplastic cellularity varied widely, from 10% to 95% (mean = 61%). All cases showed a mixed inflammatory infiltrate composed of lymphocytes and plasma cells, often with histiocytes and eosinophils. Lymphocytes and plasma cells predominated in 11 and 2 cases, respectively. One case showed adjacent mucosal ulceration (case 7) in the absence of prior therapy.

The tumor cells had a moderate amount of pale eosinophilic, lightly vacuolated cytoplasm, occasionally eccentrically located, with 2 cases showing distinct granular cell change. Nuclei were oval with smooth nuclear contours, pale, dispersed chromatin, and nucleoli that ranged from inconspicuous to prominent. Approximately half of the cases (6/13) showed intranuclear inclusions, and 5 cases showed

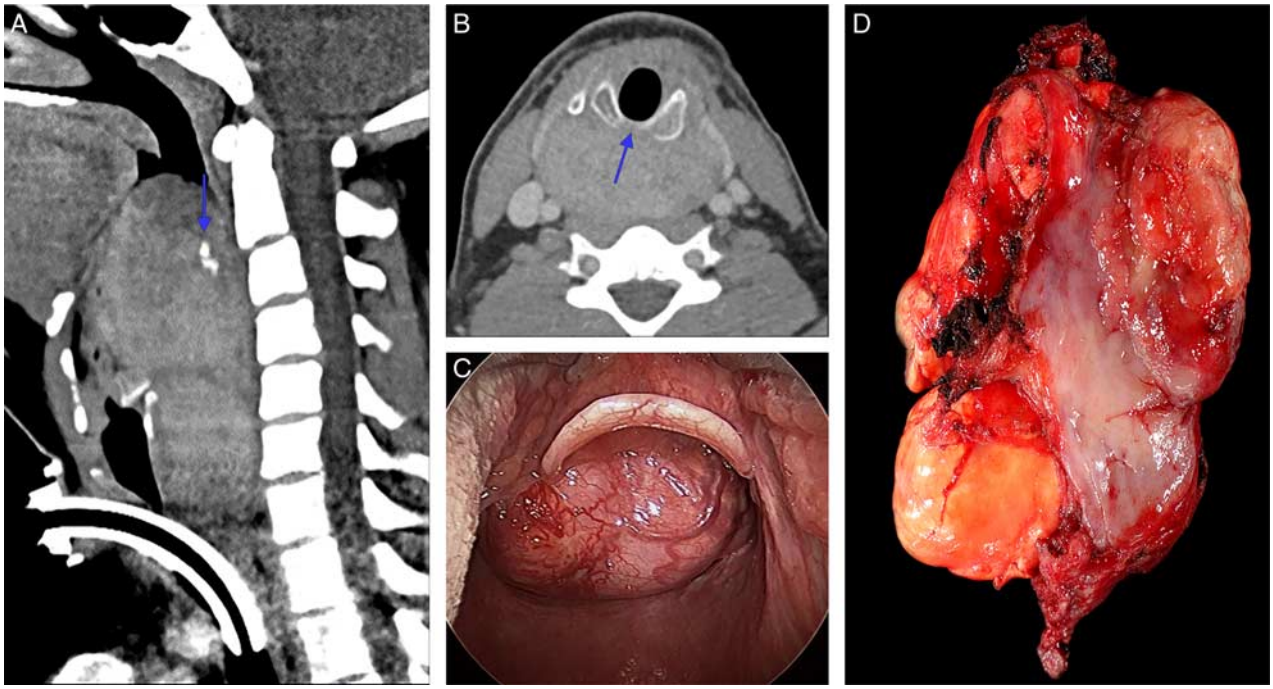

FIGURE 1. Pretreatment radiologic and laryngoscopic features of hypopharyngeal IMT with a novel *SLC12A2-ROS1* fusion (case 8). A and B, Sagittal and axial images from a contrast-enhanced neck CT scan demonstrate an enhancing 4.2×10.6 cm hypopharyngeal mass that completely fills the hypopharynx and supraglottic larynx. Note several coarse calcifications within the mass (arrow, A) and erosion of the cricoid cartilage (arrow, B). C, Direct laryngoscopy shows a well-encapsulated, lobular mass that appears to arise from the region of the left posterior cricoid and pyriform sinus with an uninvolved larynx. D, The resection specimen obtained 2 months after initiation of crizotinib therapy showed a lobular mass with soft, yellow regions indicative of necrosis and surface ulceration.

TABLE 1. Clinical Features of Head and Neck IMTs

Case #	Age (y)	Sex	Symptoms	Length of Symptoms (mo)	Exact Site	Treatment	Surgical Margin Status	Status at Last Follow-up	Follow-up Interval (y)
1	26	M	Hoarseness	3	Larynx, true vocal cord	Excisional	NA	NED	7.2
2	39	M	Marble-feeling in back of tongue	108	Oral cavity, tongue	Excisional	Neg	LR (3 y)	5.3
3	69	M	Laryngitis with hoarseness	3	Larynx, subglottis	Excisional	NA	NED	5.2
4	46	F	Changes in hearing	8	Bone, mastoid	Incisional	NA	NED	2.1
5	8	F	Hoarseness and change in voice	4	Larynx, subglottis	Excisional	NA	NED	2.1
6	25	F	Hoarseness with persistent cough	1	Larynx, true vocal cord	Excisional	NA	NED	1.3
7	14	F	SOB, loud breathing (stridor, dyspnea)	2	Larynx, subglottis	Incisional, laser ablation	NA	NED	1.5
8	28	M	Dysphagia, loss of voice, hoarseness, hemoptysis	960	Pharynx, hypopharynx	Incisional, crizotinib, then resection	Pos	NED	2
9	9	M	Small mass (dentist noted)	4	Oral cavity, lower lingual mucosa	Incisional, then excisional	Pos	NED	1.2
10	7	F	Hoarseness	0.5	Oral cavity, tongue	Incisional, then crizotinib	Pos	NED	1.8
11	33	M	Hoarseness, coughing, hemoptysis	6	Larynx, true vocal cord	Incisional	NA	U/K	U/K
12	10	M	Mild hearing loss, noisy breathing in night	60	Pharynx, oropharynx	Excisional	NA	NED	3.6
13	31	F	Hoarseness	U/K	Larynx, true vocal cord	Excisional	Pos	U/K	U/K

F indicates female; LR, local recurrence; M, male; NA, not available; NED, no evidence of disease; Neg, negative; Pos, positive; SOB, shortness of breath; U/K, unknown.

ganglion-like cells. Mitoses ranged from 0 to 5 per 2 mm^2 (median of 1/2 mm^2), and no case demonstrated atypical mitoses. No case had pretreatment necrosis, lymphovascular invasion, or marked pleomorphism. See Table 2 and Figure 3 for histologic details.

By IHC, 11/13 tumors were positive for ALK, 7/11 for SMA, 2/13 for desmin, 1/5 for MSA, and 1/4 for CD34. ROS1 IHC was retrospectively performed in 1 case with a *ROS1* fusion by molecular analysis and was negative; this was repeated in a second laboratory and showed rare positive cells. None expressed pan-keratin (n = 11), S100 protein (n = 10), p63 (n = 3), or SOX10 (n = 2). Various selected findings are outlined in Table 3 and illustrated in Figure 3.

Molecular Analysis

FISH was positive for *ALK* rearrangement in 4/4 cases (all positive for ALK IHC). All cases underwent analysis by an NGS assay; in the 12 cases that were specifically analyzed for this study, the Archer platform was used, whereas in case 8, whole-exome and whole-transcriptome NGS had previously been performed for clinical purposes. A fusion was detected in 92% (n = 11/12) cases with sufficient nucleic acid material available to complete the analysis, involving *ALK* in 10 cases and *ROS1* in 1 case. One case (case 3) failed testing due to poor RNA quality (but was positive for ALK by IHC) and another (case 4) lacked any databased fusion (and was negative for ALK by IHC). *TIMP3-ALK* represented the most common fusion (55%, n = 6/11). Additional rearrangements included 1 case each of *TPM3-ALK*, *KIF5B-ALK*, *CARS-ALK*, *THBS1-ALK*, and *SLC12A2-ROS1*. An abnormal FISH pattern was detected in 88 (44.0%) of 200 interphase nuclei analyzed featuring 1 normally juxtaposed, nonrearranged 5′*ROS1*/3′*ROS1* (green/orange) signal accompanied by 1 to 2 isolated orange signals representing the 3′ portion flanking the area from which breakpoints have been observed involving the *ROS1* gene (Fig. 4). Molecular features are summarized in Table 3.

Of the initial cohort, 1 case appeared histologically distinct from the others and was reclassified after molec-

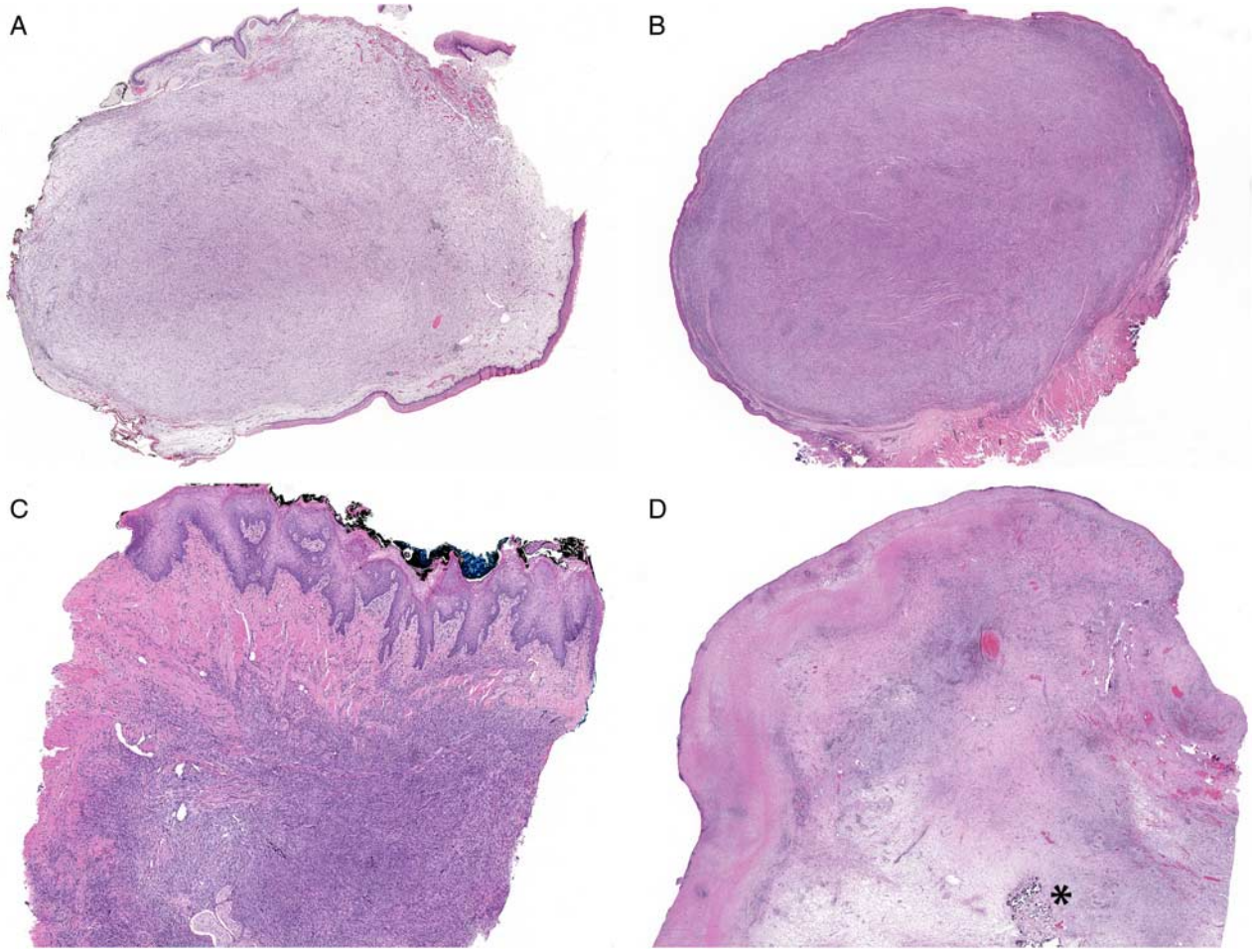

FIGURE 2. Low-power images demonstrating the growth patterns of head and neck IMT. A and B, Tumors are frequently polypoid, and half are well-circumscribed. C, Half of the tumors are infiltrative. D, The large hypopharyngeal tumor (case 8) treated with neoadjuvant crizotinib demonstrates surface ulceration and necrosis at resection. Focal calcification (*) correlates with preoperative imaging.

ular and additional IHC analysis. It was found to harbor a *FUS-TFCP2* rearrangement previously described in spindle cell rhabdomyosarcoma involving bone[18,19]; see the Discussion section (below).

Clinical Treatment and Follow-up

Most patients were treated with excision. Two patients received crizotinib therapy after biopsy. In 1 case (case 10), crizotinib therapy was administered following incisional biopsy and led to a decrease in radiographic size after 1 year with no evidence of disease recurrence after 1.5 years; therapy was stopped due to side effects (peripheral edema). In the other case (case 8, Fig. 3G), which harbored a *ROS1* fusion, crizotinib was administered over the course of 2 months. The patient experienced symptom improvement in 2 weeks with minimal toxicity, and the tumor demonstrated a radiographic decrease in size (from 10.6 to 7 cm) with central necrosis; subsequent surgical excision was performed with histologic treatment effect estimated to be 70%. One patient (case 7) received carbon dioxide laser treatment after incisional biopsy, and subsequent reexcision showed granulation tissue only. Clinical follow-up was available for 11/13 patients and ranged from 1.2 to 7.2 years (mean = 3.0 y, median = 2.1 y). One patient developed local recurrence 3 years after initial diagnosis by excisional biopsy (case 2) and is currently free of disease 5.3 years from the presentation. No patient developed metastasis.

DISCUSSION

IMT is a distinctive, relatively uncommon mesenchymal neoplasm with ~150 to 200 cases diagnosed annually in the United States.[20] Head and neck involvement is rare, with the larynx the most commonly affected subsite. Recent studies have demonstrated that IMT is largely an RTK-driven neoplasm.[2,8] In select cases, molecular analysis may capture genetic alterations that would suggest targeted therapy options to help control disease or facilitate surgery when used as neoadjuvant therapy.

In our series, we identified a putative molecular driver in 92% (n = 11/12) by NGS, and an additional case that failed NGS was ALK-positive by IHC. ALK IHC demonstrated complete concordance with FISH (n = 4) and NGS (n = 11) results. All cases with *ALK* fusions were also positive for ALK by IHC; conversely, all cases positive for ALK by IHC had a fusion partner detected by NGS, except 1 case where the test failed due to poor RNA quality (case 3). The material was unavailable to attempt ALK FISH in this case. It should be noted that false positives and negatives are possible with ALK IHC in IMT.[2,15] Several different ALK antibody clones are available, and prior studies have reported improved ALK detection using the more sensitive ALK antibody clones D5F3 or 5A4.[1,12,21] In the broader literature, some ALK IHC patterns are known to correlate with particular fusion partners.[1] We did not detect a specific staining pattern associated with *TIMP3-ALK*, the most commonly seen translocation. ROS1 IHC has also proven to be a useful tool in the diagnosis of *ROS1*-rearranged IMTs, though potentially less reliable than ALK with numerous false negatives reported.[8,12,17,22] Indeed, ROS1 IHC was negative in the single *ROS1*-rearranged IMT in our cohort in 1 laboratory and showed rare positive cells when repeated in a second laboratory using the same clone with different dilutions (Table 3).

The proportion of IMTs that harbor molecular alterations in the current study (92%) is somewhat higher than the 50% to 70% range generally reported in the literature, though it may be comparable to the 85% reported by Lovly et al.[2] We suspect that the reasons are multifactorial, including strictness of diagnostic criteria, robustness and choice of molecular testing, and cohort size and patient age. Although only 5 patients were of pediatric age in our study, just 2 were above 40 years, where *ALK* rearrangements are uncommon.[1,2]

TABLE 2. Histologic Features of Head and Neck IMTs

			Histologic Patterns (%)			
Case #	Size (cm)	Margin	Myxoid	Compact	Hyalinized	Inflammation (Amount)
1	0.6	NA	95	5	0	2+
2	1.2	W	30	70	0	3+
3	2	W	50	50	0	3+
4	2.1	NA	0	100	0	3+
5	1.6	NA	0	100	0	3+
6	1.1	NA	90	10	0	3+
7	1.5	NA	60	40	0	3+
8	10.6	W	0	100	0	2+
9	1.5	I	20	60	20	2+
10	1.1	I	0	100	0	3+
11	1.4	I	20	80	0	3+
12	2.8	U/K	0	100*	0	3+
13	0.6	W	40	60	0	2+

*Case classified as entirely compact based on best fit with the 3 classic histologic patterns, but may represent a distinct pattern where lesional cells are nearly entirely obscured by inflammation on standard histology.

2+ indicates moderate inflammation (visible at ×100); 3+, marked inflammation (visible at ×40); diffuse, diffuse inflammation (≥ 50%); I, ill-defined margin; limited, limited inflammation (< 50%); lymph, lymphocyte; N, no; plasma, plasma cell; W, well-defined margin; Y, yes.

In this series of head and neck IMTs, *TIMP3-ALK* represented the most common fusion, seen in approximately half (n = 6) of our fusion-positive cohort. Thus far, we are aware of only 1 head and neck IMT reported with this fusion (larynx).[23] However, the *TIMP3-ALK* rearrangement has recently emerged as an alteration highly characteristic in uterine and placental IMTs, frequently with a transient or indolent clinical course.[24–26] There were no identified clinicopathologic characteristics distinctive to the *TIMP3* fusion partner in this series; whether this fusion partner may additionally have a predilection for the head and neck region is a finding requiring further investigation. The other fusions were identified in only 1 case each. On the basis of the broader IMT literature, the *TPM3-ALK* fusion is the most common IMT fusion we identified in this series.[2,27,28] *KIF5B-ALK* has been reported in an 11-year-old girl with a central nervous system tumor.[29] Like the other *ALK* fusion partners, *KIF5B* was initially reported as an *ALK* translocation partner in non–small cell carcinoma of the lung,[30] where it is relatively common.[31] This alteration is emerging as a characteristic, recurrent fusion in ALK-positive histiocytosis, an unusual histiocytosis variant with a predilection for infants and young children[32] that has very recently also been reported in adults (see below).[33] *CARS-ALK* has also been reported in 2 IMTs to date, including 1 with subsequent lung metastasis.[34,35]

We identified a novel rearrangement in IMT, *SLC12A2-ROS1* (Fig. 5), which was evident by 3 different approaches (whole-exome sequencing, whole-transcriptome sequencing, and *ROS1* FISH). The *ROS1* FISH pattern showed predominantly isolated 3′ signals, a finding previously described in *ROS1*-rearranged IMT.[22] While ROS1 is a well-established proto-oncogene RTK and corresponding *ROS1* gene rearrangements are present in ~10% of IMTs,[1,8,9] the *SLC12A2* partner had not been previously been reported in cancer; following the submission of this manuscript, a *SLC12A2-ROS1* fusion was reported in a lung adenocarcinoma responsive to crizotinib.[36] The recently documented fusion involved exon 15 of *SLC12A2* and exon 36 of *ROS1*,[36] whereas the present case involves exon 14 of *SLC12A2* and exon 35 of *ROS1*. While data is limited regarding this *ROS1* fusion partner, a related solute carrier family member, *SLC34A2*, was established as a *ROS1* fusion partner in pulmonary non–small cell carcinoma.[37,38] The mechanism by which ROS1 fusion proteins become constitutively active is unknown.[39] Given available evidence and close parallels with the patterns seen in lung cancer,[8,40] this novel fusion kinase likely causes constitutive activation and drives cellular transformation. Indeed, the significant response to neoadjuvant crizotinib therapy in both reported *SLC12A2-ROS1*-fused tumors supports this driver function of the fusion product.

The 1 case that was successfully interrogated by a targeted RNA NGS assay and lacked an identifiable fusion (case 4) represented a mastoid bone tumor in a 46-year-old woman. Histologically, the tumor demonstrated characteristic morphologic features of IMT (Fig. 3D) but was negative for ALK IHC. Additional IHC studies supported the morphologic impression of myofibroblastic differentiation (SMA positive) while being negative for MSA, desmin, pan-keratin, p63, S100 protein, and CD21. This case was analyzed by the v4 Archer platform which does not cover some of the rarely reported IMT fusions (such as *PDGFRB* and *RET*),[2,8] so it is possible that a known driver molecular alteration was not tested.

The differential diagnosis of IMT is broad and depends on the predominant morphologic features. Sarcomatoid or spindle cell squamous cell carcinoma is a significantly more common spindle cell upper aerodigestive tract neoplasm that can overlap with IMT; both may present as polypoid laryngeal masses, have a myxoid matrix, and show myogenic differentiation. Surface dysplasia, zones of transition, and immunoreactivity for epithelial markers, p40/p63, or strong p53 expression support carcinoma. While these features are present in the majority of spindle cell carcinomas, they are not invariably seen. Additional morphologic clues supporting

TABLE 2. (*Continued*)

Inflammation (Distribution)	Predominant Inflammatory Cell	Lesional Cellularity (%)	Intranuclear Inclusions Present	Ganglion-like Cells Present	Granular Cell Change Present	Mitoses (# Per 2 mm^2)
Limited	Lymph	70	N	Y	N	1
Diffuse	Lymph	70	N	Y	N	2
Limited	Lymph	50	Y	Y	N	1
Diffuse	Plasma	30	N	N	N	1
Limited	Lymph	70	N	N	N	2
Diffuse	Lymph = plasma	50	Y	Y	N	1
Limited	Lymph	80	N	Y	N	1
Limited	Lymph	80	Y	N	Y	1
Limited	Lymph	70	Y	N	N	2
Limited	Lymph	90	N	N	N	5
Diffuse	Lymph	50	Y	N	Y	0
Limited	Plasma	10	N	N	N	0
Limited	Lymph	80	Y	N	N	0

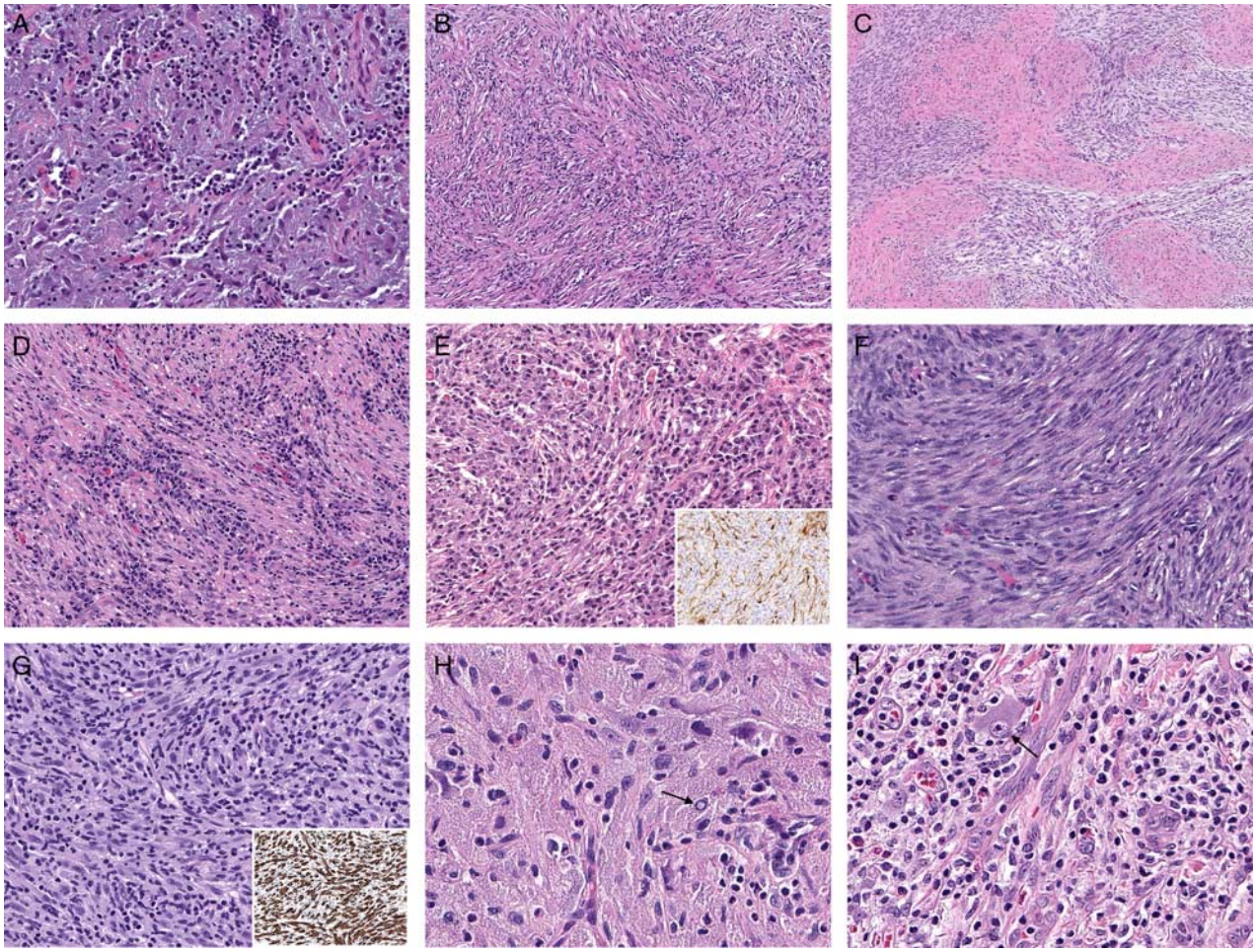

FIGURE 3. Histologic and immunophenotypic features of IMT of the head and neck. A, The myxoid pattern shows loosely arranged spindle-shaped tumor cells suspended in a pale blue matrix with prominent background vascularity (case 1). B, The compact pattern shows a cellular proliferation of spindle cells in storiform arrangements (case 5). C, Fascicular growth may also be seen in cases with a compact pattern; here this pattern alternates with areas of the dense collagenous pattern, evident as regions of hypocellular collagen with few spindle cells. A prior biopsy was interpreted as traumatic fibroma due to predominant sampling of this component (case 9). D, In most cases, chronic inflammation is readily identified at low power (case 4). E, Neoplastic cellularity varies widely and can be very low; here plasma cells almost entirely obscure the underlying lesional spindle cells (inset: ALK IHC highlights scattered lesional spindle cells case 12). F, Other cases show high cellularity with few inflammatory cells (case 10). G, Most tumors demonstrate a cytologically bland, uniform population of spindle cells that are positive for 1 or more myogenic marker by IHC (inset: desmin IHC demonstrates strong reactivity in tumor cells, case 8). H, Approximately half of cases show intranuclear inclusions (arrow), and granular change can be seen (case 11). I, Ganglion-like tumor cells represent a common finding (arrow, case 2).

spindle cell carcinoma include moderate to severe nuclear atypia with hyperchromasia, hypercellularity, atypical mitotic figures, and more prominent/nearly universal surface ulceration. Clinically, spindle cell carcinoma patients are more likely to be older (sixth to eighth decades), male (85%), have tobacco or alcohol use, and have a history of prior radiation therapy. Molecular analysis may help, as spindle cell carcinoma shows complex genetic alterations and lacks *ALK*- or related gene rearrangements seen in many IMTs.[41]

Mesenchymal neoplasms, in particular, spindle cell neoplasms with myogenic differentiation also enter the differential. Indeed, this was true of the 1 case in our initial prospective cohort that was excluded after molecular analysis. A *FUS-TFCP2* fusion was identified in a case initially diagnosed as a hard palate IMT in a 23-year-old man, which presented as a destructive, infiltrative mass involving the maxilla and nasal cavity. This case was positive for ALK by IHC. However, the identification of a *FUS-TFCP2* fusion prompted reevaluation. This fusion has been reported in spindle cell rhabdomyosarcoma,[18,19] a tumor with a predilection for craniofacial bones and frequent ALK overexpression in the absence of *ALK* fusion by NGS or FISH.[42] We subsequently performed IHC studies for myogenin (MYF4) and MyoD1, both of which

TABLE 3. IHC and Molecular Features of Head and Neck IMTs

Case #	SMA IHC	Desmin IHC	ALK IHC	ALK Antibody Clone*	ALK IHC Pattern	ALK FISH	Fusion Gene Identified†
1	N	N	P	ALK01	Cytoplasmic: granular and perinuclear accentuation	NP	*TIMP3* (exon 1)-*ALK* (exon 19)
2	N	N	P	ALK01	Cytoplasmic: granular and perinuclear accentuation	NP	*TIMP3* (exon 1)-*ALK* (exon 19)
3	P	N	P	ALK01	Cytoplasmic: granular	NP	Failed
4	P	N	N	ALK01	N	NP	No fusion
5	P	N	P	ALK01	Cytoplasmic: granular	NP	*KIF5B* (exon 24)-*ALK* (exon 20)
6	NP	N	P	ALK01	Cytoplasmic: diffuse	NP	*TIMP3* (exon 3)-*ALK* (exon 18)
7	P	N	P	ALK1	Cytoplasmic: granular	NP	*TIMP3* (exon 1)-ALK (exon 19)
8‡	P	P	N	5A4 and D5F3	N	NP§	*SLC12A2* (exon 14)-*ROS1* (exon 35)
9	N	N	P	ALK1	Cytoplasmic: diffuse	P	*TPM3* (exon 8)-*ALK* (exon 20)
10	P	N	P	ALK1	Cytoplasmic: variable weak	P	*CARS* (exon 17)-*ALK* (exon 20)
11	N	N	P	5A4	Cytoplasmic: granular	P	*TIMP3* (exon 3)-*ALK* (exon 18)
12	NP	N	P	5A4	Cytoplasmic: granular	P	*THBS1* (exon 7)-*ALK* (exon 19)
13	P	P (rare)	P	D5F3	Cytoplasmic: granular	NP	*TIMP3* (exon 1)-*ALK* (exon 19)

*ALK IHC details: clone ALK01 (RTU dilution; Ventana Medical Systems, Tucson, AZ); clone ALK1 (Dako, Carpinteria, CA); 1:10 dilution; clone 5A4 (1:100 dilution for cases 8 and 11 and 1:50 dilution for case 12; Novocastra, Leica Biosystems, Buffalo Grove, IL); clone D5F3 (1:50 dilution for case 8 and 1:100 dilution for case 13; Cell Signaling Technology, Danvers, MA).

†NGS fusion assay details: case 3, poor RNA quality; case 8: whole-transcriptome and whole-exome NGS; case 13: Archer FusionPlex Sarcoma Panel, v5; all remaining cases: Archer FusionPlex Sarcoma Panel, v4.

‡ROS1 IHC (clone D4D6; Cell Signaling Technology) was performed in case 8 and was negative in 1 laboratory (1:200 dilution) and showed rare positive cells in a separate laboratory (1:50 and 1:25 dilutions).

§ROS1 FISH was performed and was positive.

N indicates negative; NP, not performed; P, positive.

were positive, confirming the diagnosis of spindle cell rhabdomyosarcoma (Fig. 6). In addition, *ALK* FISH was performed by 2 separate laboratories and showed an atypical pattern consisting of homozygous loss of the 5′ green signal. ALK expression has been previously reported in rhabdomyosarcoma and the mechanism is a de novo alternative transcription initiation (ATI) site in ALK intron 19, termed ALK(ATI).[42,43] ALK(ATI) is biallelically expressed, and recurrent genetic aberrations at the ALK locus are not present.[43] The *ALK* FISH probes are designed to flank the *ALK* exon 20 recurrent breakpoint; we hypothesize that the biallelic expression of the ALK(ATI) transcript explains the homozygous loss of the 5′ green signal in this case. This is a potential pitfall when evaluating ALK status by IHC or FISH in rhabdomyosarcoma when the differential diagnosis is IMT. Furthermore, the morphologic overlap between these entities is significant, with limited atypia in spindle cell rhabdomyosarcoma, while IMTs may demonstrate cytologic atypia in the absence of aggressive biological behavior. Strong, diffuse desmin expression is more typical of rhabdomyosarcoma than IMT, though this

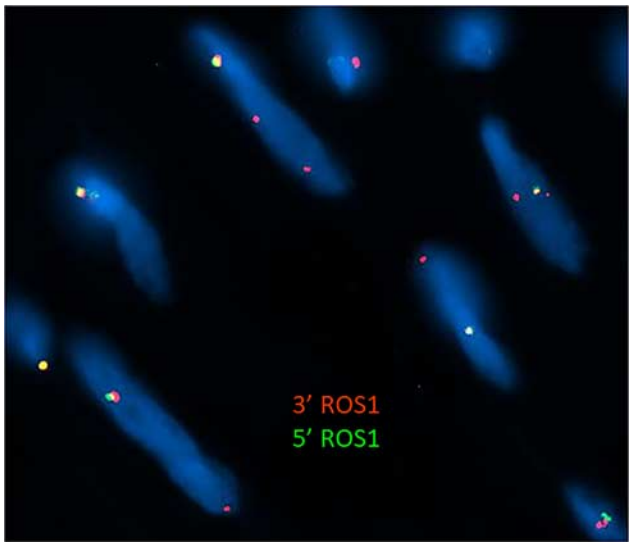

FIGURE 4. FISH showing cells with a juxtaposed (non-rearranged) orange/green signal accompanied by 1 to 2 isolated *ROS1* 3′ (orange) signals.

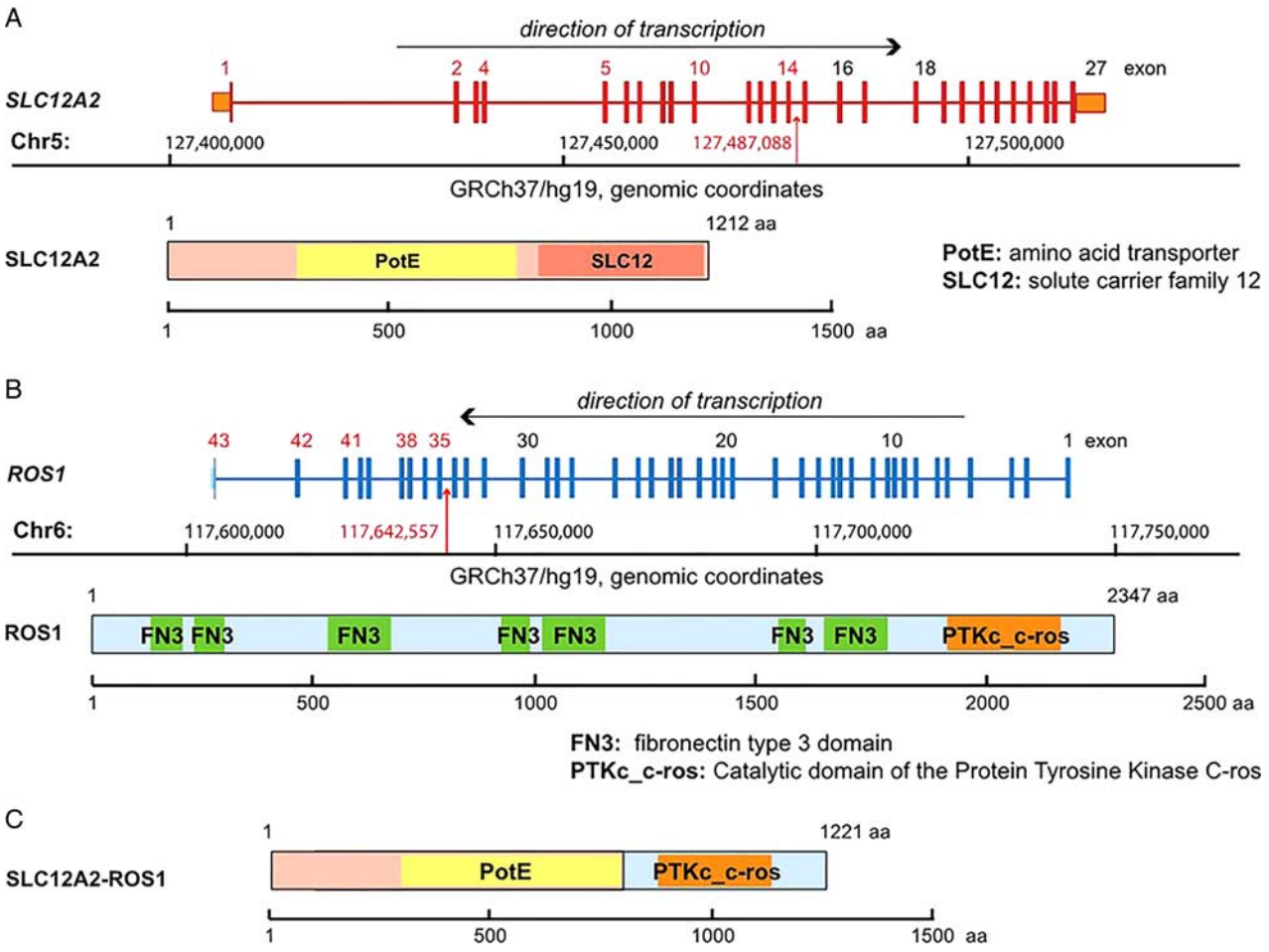

FIGURE 5. Schematic representation of the novel *SLC12A2-ROS1* fusion. A, Genomic location and the exon/intron structure of the *SLC12A2* gene and the functional domains of the encoded SLC12A2 protein. The exons are numbered; exons involved in the *SLC12A2-ROS1* fusion are in red. B, Genomic location and the exon/intron structure of the *ROS1* gene (exons involved in the fusion are numbered in red) and the functional domains of the encoded ROS1 protein. The red arrows designate the location of the genomic breakpoints with the coordinates as indicated by NGS. C, The SLC12A2-ROS1 predicted fusion protein of 1221 aa.

feature is not universal or discriminatory.[42] Routine inclusion of myogenin and MyoD1 in the IHC workup of ALK-positive spindle cell tumors should be considered, with judicious use of molecular diagnostics when feasible.

Dedifferentiated liposarcoma is another spindle cell neoplasm with myogenic differentiation that enters the differential, exceptional though potentially underrecognized in the head and neck.[44] It can harbor admixed inflammatory cells with regions exhibiting low-grade cytomorphologic features. MDM2 immunoreactivity is not discriminatory as nuclear staining is commonly observed in IMT.[6,7] Identification of a well-differentiated lipomatous component and/or detection of *MDM2* amplification by FISH can confirm the diagnosis.[44,45] *Inflammatory rhabdomyoblastic tumor* is a recently proposed term to describe a group of tumors designated as *inflammatory leiomyosarcoma* or *histiocyte-rich rhabdomyoblastic tumor*.[46,47] These tumors tend to occur in the extremities of young to middle-aged adults and are composed of spindle to epithelioid cells with a histiocyte-rich chronic inflammatory infiltrate. Immunophenotypically, the cells express rhabdomyoblastic markers (myogenin, MyoD1, and PAX7),[46,47] whereas IMTs are negative for these markers.[48] They harbor a distinct molecular profile characterized by near-haploidization and high expression of genes involved in smooth and skeletal muscle development.[49]

The admixture of spindle cells and chronic inflammation seen in IMT can also raise the differential diagnosis of histiocytic and dendritic cell neoplasms. Follicular dendritic cell sarcoma can express desmin in ~10% of cases, rarely in a strong and diffuse fashion, but inevitably express follicular dendritic cell markers such as CD21 and or CD35.[50] Interdigitating dendritic cell sarcomas are consistently positive for S100 protein, which is typically negative in IMT.[6] ALK-positive histiocytosis has a potentially overlapping immunophenotype with IMT

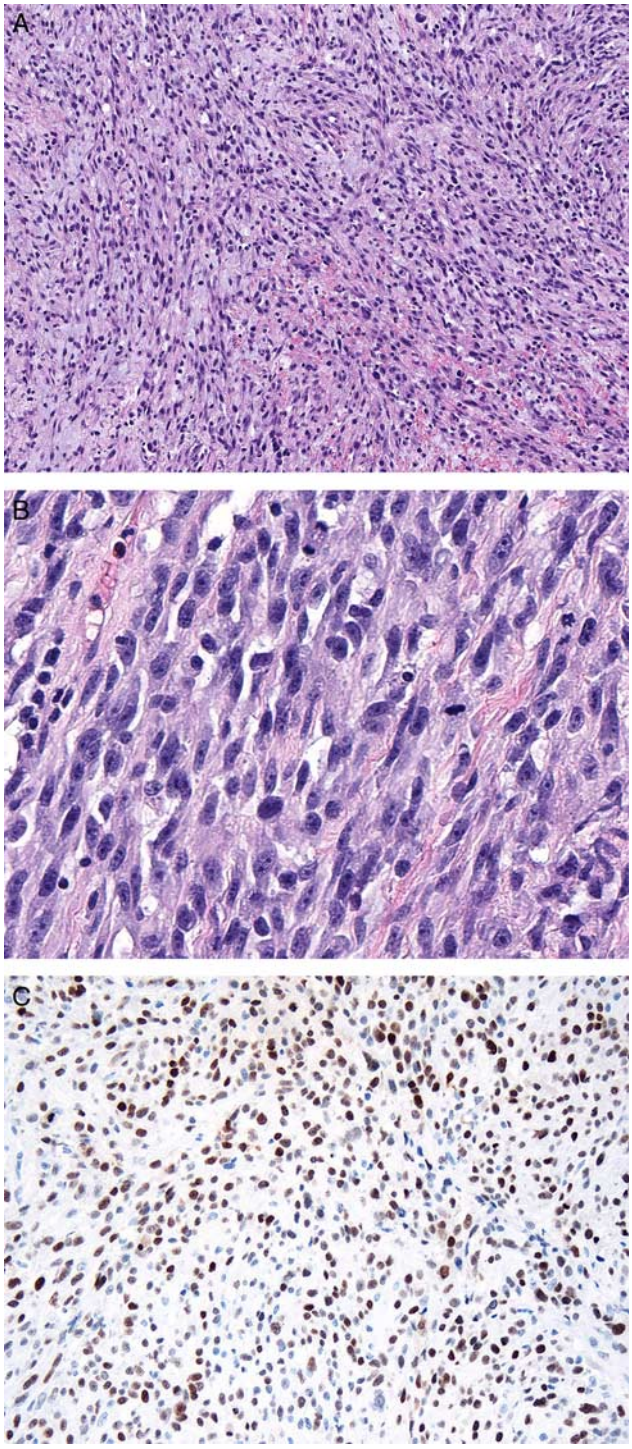

FIGURE 6. Morphologic and immunophenotypic features of the excluded case reclassified as spindle cell rhabdomyosarcoma with *FUS-TFCP2* rearrangement. A, Low-power view shows a moderately cellular spindle cell neoplasm with a collagenous to myxoid stroma and scattered chronic inflammatory cells. The tumor cells were positive for ALK by IHC (not shown). B, Cytologically the tumor cells demonstrate moderate nuclear atypia. Scattered mitotic figures are present. C, Many tumor cells are positive for MyoD1 by IHC, supporting the diagnosis of rhabdomyosarcoma.

but has historically been regarded as morphologically distinct, a neoplasm of large, epithelioid histiocytes with ample eosinophilic cytoplasm and folded nuclei.[32] However, a recent report of 3 cases presenting as breast masses in adolescent and adult patients emphasized the possibility of predominant spindle cell morphology in these tumors, rendering significant overlap with IMT. Features that support a diagnosis of ALK-positive histiocytosis include the presence of foci displaying conventional epithelioid morphology or admixed Touton-type giant cells, and scrutiny of the IHC pattern may be able to help identify the ALK-positive neoplastic cells as CD163-positive histiocytes, separate from SMA-positive reactive myofibroblasts. This is an emerging entity with only 18 reported cases in the literature thus far, though it is likely underrecognized, with ALK-rearranged histiocytic tumors reported under various diagnostic terms in various anatomic sites including the head and neck; future studies may provide additional insight.[33]

For highly inflamed tumors, the differential diagnosis for IMT includes reactive and/or inflammatory pseudotumoral processes. In the larynx, vocal cord nodules can show areas reminiscent of IMT but are separated by their small size, restriction to Reinke space (the glottic subspecialized mucosa), and lack of characteristic molecular alterations. A series of highly inflamed IMTs (case 12 in this series) highlights the potential for overlap with IgG_4-related disease based on morphology and IgG_4 IHC; as such, judicious use of ALK and ROS1 IHC with consideration of NGS is suggested.[17]

In summary, our results add to the growing body of evidence that kinase fusions can be identified in the majority of IMTs, helping to further define this entity as a predominantly TRK-driven disease process. IMTs notoriously display a wide spectrum of morphologies, and this was well-illustrated in our cohort of head and neck IMTs. We identified *TIMP3-ALK* as the most common fusion in head and neck IMTs, raising the possibility that this particular alteration may show a predilection for this anatomic region. We also identified a novel fusion, *SLC12A2-ROS1*, in a crizotinib-responsive IMT of the hypopharynx in a 28-year-old man, expanding the spectrum of genetic alterations identified in this disease. Further, this case highlights the judicious use of NGS to facilitate the management, potentially decreasing morbidity. While no patient in our cohort experienced metastatic disease and only 1 tumor locally recurred, it is possible that longer clinical follow-up intervals may be necessary to fully understand the biological potential of these neoplasms, though this data generally conforms to that reported in other sites. Judicious use of NGS can help identify RTK fusion-positive IMTs, which may provide potential treatment options for selected patients and help avoid diagnostic pitfalls such as the case of ALK-positive spindle cell rhabdomyosarcoma illustrated herein.

ACKNOWLEDGMENTS

The authors thank Dr Janos Sumegi for his assistance in preparing the molecular figure (Fig. 5) and Johanna Mabray for her technical assistance.

REFERENCES

1. Yamamoto H. Inflammatory myofibroblastic tumour. In: WHO Classification of Tumours Editorial Board, ed. *Soft Tissue and Bone Tumours*. Lyon, France: International Agency for Research on Cancer; 2020:109–111.
2. Lovly CM, Gupta A, Lipson D, et al. Inflammatory myofibroblastic tumors harbor multiple potentially actionable kinase fusions. *Cancer Discov*. 2014;4:889–895.
3. Tao J, Zhou M-L, Zhou S-H. Inflammatory myofibroblastic tumors of the head and nec. *Int J Clin Exp Med*. 2015;8:1604–1610.
4. Coffin CM, Watterson J, Priest JR, et al. Extrapulmonary inflammatory myofibroblastic tumor (inflammatory pseudotumor). A clinicopathologic and immunohistochemical study of 84 cases. *Am J Surg Pathol*. 1995;19:859–872.
5. Mariño-Enríquez A, Wang W-L, Roy A, et al. Epithelioid inflammatory myofibroblastic sarcoma: an aggressive intra-abdominal variant of inflammatory myofibroblastic tumor with nuclear membrane or perinuclear ALK. *Am J Surg Pathol*. 2011;35:135–144.
6. Gleason BC, Hornick JL. Inflammatory myofibroblastic tumours: where are we now? *J Clin Pathol*. 2008;61:428–437.
7. Coffin CM, Hornick JL, Fletcher CDM. Inflammatory myofibroblastic tumor: comparison of clinicopathologic, histologic, and immunohistochemical features including ALK expression in atypical and aggressive cases. *Am J Surg Pathol*. 2007;31:509–520.
8. Antonescu CR, Suurmeijer AJH, Zhang L, et al. Molecular characterization of inflammatory myofibroblastic tumors with frequent ALK and ROS1 gene fusions and rare novel RET rearrangement. *Am J Surg Pathol*. 2015;39:957–967.
9. Preobrazhenskaya EV, Iyevleva AG, Suleymanova AM, et al. Gene rearrangements in consecutive series of pediatric inflammatory myofibroblastic tumors. *Pediatr Blood Cancer*. 2020;67:e28220.
10. Cook JR, Dehner LP, Collins MH, et al. Anaplastic lymphoma kinase (ALK) expression in the inflammatory myofibroblastic tumor: a comparative immunohistochemical study. *Am J Surg Pathol*. 2001;25:1364–1371.
11. Cessna MH, Zhou H, Sanger WG, et al. Expression of ALK1 and p80 in inflammatory myofibroblastic tumor and its mesenchymal mimics: a study of 135 cases. *Mod Pathol*. 2002;15:931–938.
12. Yamamoto H, Yoshida A, Taguchi K, et al. ALK, ROS1 and NTRK3 gene rearrangements in inflammatory myofibroblastic tumours. *Histopathology*. 2016;69:72–83.
13. Piarulli G, Puls F, Wängberg B, et al. Gene fusion involving the insulin-like growth factor 1 receptor in an ALK-negative inflammatory myofibroblastic tumour. *Histopathology*. 2019;74:1098–1102.
14. Butrynski JE, D'Adamo DR, Hornick JL, et al. Crizotinib in ALK-rearranged inflammatory myofibroblastic tumor. *N Engl J Med*. 2010;363:1727–1733.
15. Bennett JA, Nardi V, Rouzbahman M, et al. Inflammatory myofibroblastic tumor of the uterus: a clinicopathological, immunohistochemical, and molecular analysis of 13 cases highlighting their broad morphologic spectrum. *Mod Pathol*. 2017;30:1489–1503.
16. Dobin A, Davis CA, Schlesinger F, et al. STAR: ultrafast universal RNA-seq aligner. *Bioinformatics*. 2013;29:15–21.
17. Taylor MS, Chougule A, MacLeay AR, et al. Morphologic overlap between inflammatory myofibroblastic tumor and IgG4-related disease: lessons from next-generation sequencing. *Am J Surg Pathol*. 2019;43:314–324.
18. Dashti NK, Wehrs RN, Thomas BC, et al. Spindle cell rhabdomyosarcoma of bone with FUS-TFCP2 fusion: confirmation of a very recently described rhabdomyosarcoma subtype. *Histopathology*. 2018;73:514–520.
19. Watson S, Perrin V, Guillemot D, et al. Transcriptomic definition of molecular subgroups of small round cell sarcomas. *J Pathol*. 2018;245:29–40.
20. Tothova Z, Wagner AJ. Anaplastic lymphoma kinase-directed therapy in inflammatory myofibroblastic tumors. *Curr Opin Oncol*. 2012;24:409–413.
21. Takeuchi K, Soda M, Togashi Y, et al. Pulmonary inflammatory myofibroblastic tumor expressing a novel fusion, PPFIBP1-ALK: reappraisal of anti-ALK immunohistochemistry as a tool for novel ALK fusion identification. *Clin Cancer Res*. 2011;17:3341–3348.
22. Hornick JL, Sholl LM, Dal Cin P, et al. Expression of ROS1 predicts ROS1 gene rearrangement in inflammatory myofibroblastic tumors. *Mod Pathol*. 2015;28:732–739.
23. Yorita K, Togashi Y, Nakagawa H, et al. Vocal cord inflammatory myofibroblastic tumor with mucoid deposits harboring TIM-P3-ALK fusion: a potential diagnostic pitfall. *Pathol Int*. 2019;69:366–371.
24. Cheek EH, Fadra N, Jackson RA, et al. Uterine inflammatory myofibroblastic tumors in pregnant women with and without involvement of the placenta: a study of 6 cases with identification of a novel TIMP3-RET fusion. *Hum Pathol*. 2020;97:29–39.
25. Makhdoum S, Nardi V, Devereaux KA, et al. Inflammatory myofibroblastic tumors associated with the placenta: a series of 9 cases. *Hum Pathol*. 2020;106:62–73.
26. Devereaux KA, Fitzpatrick MB, Hartinger S, et al. Pregnancy-associated inflammatory myofibroblastic tumors of the uterus are clinically distinct and highly enriched for TIMP3-ALK and THBS1-ALK fusions. *Am J Surg Pathol*. 2020;44:970–981.
27. Yamamoto H, Kohashi K, Oda Y, et al. Absence of human herpesvirus-8 and Epstein-Barr virus in inflammatory myofibroblastic tumor with anaplastic large cell lymphoma kinase fusion gene. *Pathol Int*. 2006;56:584–590.
28. Lawrence B, Perez-Atayde A, Hibbard MK, et al. TPM3-ALK and TPM4-ALK oncogenes in inflammatory myofibroblastic tumors. *Am J Pathol*. 2000;157:377–384.
29. Maruggi M, Malicki DM, Levy ML, et al. A novel KIF5B-ALK fusion in a child with an atypical central nervous system inflammatory myofibroblastic tumour. *BMJ Case Rep*. 2018;2018:bcr2018226431.
30. Takeuchi K, Choi YL, Togashi Y, et al. KIF5B-ALK, a novel fusion oncokinase identified by an immunohistochemistry-based diagnostic system for ALK-positive lung cancer. *Clin Cancer Res*. 2009;15:3143–3149.
31. Du X, Shao Y, Qin H-F, et al. ALK-rearrangement in non-small-cell lung cancer (NSCLC). *Thorac Cancer*. 2018;9:423–430.
32. Chang KTE, Tay AZE, Kuick CH, et al. ALK-positive histiocytosis: an expanded clinicopathologic spectrum and frequent presence of KIF5B-ALK fusion. *Mod Pathol*. 2019;32:598–608.
33. Kashima J, Yoshida M, Jimbo K, et al. ALK-positive histiocytosis of the breast: a clinicopathologic study highlighting spindle cell histology. *Am J Surg Pathol*. 2021;45:347–355.
34. Debelenko LV, Arthur DC, Pack SD, et al. Identification of CARS-ALK fusion in primary and metastatic lesions of an inflammatory myofibroblastic tumor. *Lab Invest*. 2003;83:1255–1265.
35. Cools J, Wlodarska I, Somers R, et al. Identification of novel fusion partners of ALK, the anaplastic lymphoma kinase, in anaplastic large-cell lymphoma and inflammatory myofibroblastic tumor. *Genes Chromosomes Cancer*. 2002;34:354–362.
36. Rodríguez-Antolín C, Rosas-Alonso R, Cruz P, et al. Novel SLC12A2-ROS1 fusion in non-small cell lung cancer with a significant response to crizotinib: the importance of choosing the appropriate next-generation sequencing assay. *Oncologist*. 2021. [Epub ahead of print].
37. Shaw AT, Ou S-HI, Bang Y-J, et al. Crizotinib in ROS1-rearranged non-small-cell lung cancer. *N Engl J Med*. 2014;371:1963–1971.
38. Davies KD, Le AT, Theodoro MF, et al. Identifying and targeting ROS1 gene fusions in non-small cell lung cancer. *Clin Cancer Res*. 2012;18:4570–4579.
39. Davies KD, Doebele RC. Molecular pathways: ROS1 fusion proteins in cancer. *Clin Cancer Res*. 2013;19:4040–4045.
40. Takeuchi K, Soda M, Togashi Y, et al. RET, ROS1 and ALK fusions in lung cancer. *Nat Med*. 2012;18:378–381.
41. Heidarian A, Wenig BM. The most common mistake in laryngeal pathology and how to avoid it. *Head Neck Pathol*. 2021;15:130–137.
42. Le Loarer F, Cleven AHG, Bouvier C, et al. A subset of epithelioid and spindle cell rhabdomyosarcomas is associated with TFCP2 fusions and common ALK upregulation. *Mod Pathol*. 2020;33:404–419.
43. Wiesner T, Lee W, Obenauf AC, et al. Alternative transcription initiation leads to expression of a novel ALK isoform in cancer. *Nature*. 2015;526:453–457.

44. Fritchie K, Ghosh T, Graham RP, et al. Well-differentiated/dedifferentiated liposarcoma arising in the upper aerodigestive tract: 8 cases mimicking non-adipocytic lesions. *Head Neck Pathol*. 2020;14:974–981.
45. Wang GY, Lucas DR. Dedifferentiated liposarcoma with myofibroblastic differentiation. *arch Pathol Lab Med*. 2018;142:1159–1163.
46. Cloutier JM, Charville GW, Mertens F, et al. 'Inflammatory leiomyosarcoma' and 'histiocyte-rich rhabdomyoblastic tumor': a clinicopathological, immunohistochemical and genetic study of 13 cases, with a proposal for reclassification as 'Inflammatory Rhabdomyoblastic Tumor'. *Mod Pathol*. 2021;34:758–769.
47. Michal M, Rubin BP, Kazakov DV, et al. Inflammatory leiomyosarcoma shows frequent co-expression of smooth and skeletal muscle markers supporting a primitive myogenic phenotype: a report of 9 cases with a proposal for reclassification as low-grade inflammatory myogenic tumor. *Virchows Arch*. 2020;477:219–230.
48. Cessna MH, Zhou H, Perkins SL, et al. Are myogenin and myoD1 expression specific for rhabdomyosarcoma? A study of 150 cases, with emphasis on spindle cell mimics. *Am J Surg Pathol*. 2001;25:1150–1157.
49. Arbajian E, Köster J, Vult von Steyern F, et al. Inflammatory leiomyosarcoma is a distinct tumor characterized by near-haploidization, few somatic mutations, and a primitive myogenic gene expression signature. *Mod Pathol*. 2018;31:93–100.
50. Andersen MJ Jr, Kerr DA, Lisovsky M, et al. Fine needle aspiration of an intranodal follicular dendritic cell sarcoma: a case report with molecular analysis and review of the literature. *Diagn Cytopathol*. 2021;49:E65–E70.